Quantized Superfluid Vortex Rings in the Unitary Fermi Gas

Aurel Bulgac,[1] Michael McNeil Forbes,[2,1,3] Michelle M. Kelley,[4] Kenneth J. Roche,[5,1] and Gabriel Wlazłowski[6,1]
[1]*Department of Physics, University of Washington, Seattle, Washington 98195-1560, USA*
[2]*Institute for Nuclear Theory, University of Washington, Seattle, Washington 98195-1550, USA*
[3]*Department of Physics and Astronomy, Washington State University, Pullman, Washington 99164-2814, USA*
[4]*Department of Physics, University of Illinois at Urbana-Champaign, Il 61801-3080, USA*
[5]*Pacific Northwest National Laboratory, Richland, Washington 99352, USA*
[6]*Faculty of Physics, Warsaw University of Technology, Ulica Koszykowa 75, 00-662 Warsaw, Poland*
(Received 20 June 2013; published 16 January 2014)

In a recent article, Yefsah *et al.* [Nature (London) **499**, 426 (2013)] report the observation of an unusual excitation in an elongated harmonically trapped unitary Fermi gas. After phase imprinting a domain wall, they observe oscillations almost an order of magnitude slower than predicted by any theory of domain walls which they interpret as a "heavy soliton" of inertial mass some 200 times larger than the free fermion mass or 50 times larger than expected for a domain wall. We present compelling evidence that this "soliton" is instead a quantized vortex ring, by showing that the main aspects of the experiment can be naturally explained within the framework of time-dependent superfluid density functional theories.

DOI: 10.1103/PhysRevLett.112.025301 PACS numbers: 67.85.Lm, 03.75.Kk, 03.75.Ss, 67.85.De

Collective modes in the form of topological and dynamical defects—solitons, vortices, vortex rings, etc.—embody the emergence of nontrivial collective dynamics from microscopic degrees of freedom, and provide a challenge for many-body theories from cold atoms through electronic superconductors to nuclei and neutron stars. The unitary Fermi gas (UFG) provides an ideal strongly interacting system for measuring and testing collective modes where controlled experiments and theoretical techniques are starting to converge [1]. A handful of predicted collective modes have been directly observed, including collective oscillations of harmonically trapped gases [2,3], higher-nodal collective modes [4], scissor modes [2], quantized vortices and vortex lattices [5], shock waves [6], and phonons (speed of sound [7], critical velocity [8], and first and second sound [4,9]). Other modes, such as the Higgs mode [10,11], vortex rings [12], and domain walls [13–17], have been demonstrated in simulations, but await direct observation. In this Letter, we discuss the objects observed in [18]: they interpret these as "heavy solitons"; we show them to be vortex rings.

Experimental puzzle: Slowly moving "solitons."—The recent MIT experiment [18] measures a slowly moving soliton produced by a sharp spatially delineated phase imprint on an ultracold cloud of some 10^5 ^{6}Li atoms in an elongated harmonic trap. These solitons cannot be resolved *in situ*, but appear after a specific time-of-flight expansion procedure that includes a rapid ramp of the interaction strength which is controlled through a Feshbach resonance by an external magnetic field. In particular, they note that a certain minimum field $B_{\min} < 700$ G is required to resolve the solitons (discussed in their Supplemental Material). From the images, they extract the period of oscillation, and find that it increases as the inverse trap aspect ratio $1/\lambda$ and the magnetic field B are increased. Increasing the temperature, they observe "antidampening" whereby the amplitude of the oscillation increases with time. The authors interpret these results as the observation of a heavy soliton with a mass "more than 50 times larger than the theoretically predicted value" and "200 times their bare mass."

Topological objects in the BEC-BCS crossover.—Superfluids are characterized by a complex-valued order parameter Ψ that describes the condensate wave function in Bose-Einstein condensates (BECs) and the Cooper pair condensate in fermionic Bardeen-Cooper-Schrieffer (BCS) superfluids. The superfluid ground state picks a coherence overall phase of the complex order parameter, spontaneously breaking the original $U(1)$ phase symmetry of the theory. Sound waves manifest as fluctuations in this coherent phase (phonons or Nambu-Goldstone modes). Landau's original argument for ^{4}He superfluidity posits a kinematical critical flow velocity v_c below which neither pair-breaking nor sound excitations can be generated. This argument is spoiled by the generation of topologically stable excitations that can nucleate at the edge of the fluid, lowering the v_c. The dynamics of these topological excitations and their interactions are at the heart of quantum turbulence studies [19].

The single-valued order parameter admits several topologically stable objects in three dimensions. Domain walls separate regions of different phases while vortices correspond to the phase winding around a line along which the order parameter vanishes. In bosonic theories (BEC limit), the number density $n \propto |\Psi|^2$ vanishes in the core of vortices and in stationary domain walls, giving these objects a "negative mass. For fermions, while the complex order parameter has a similar behavior, the relationship $n \propto |\Psi|^2$ breaks down, with the interpretation that the core of the topological defects are filled with "normal" fluid, but

at unitarity the number density depletion is still substantial [12,20,21]. A manifestation of this negative mass is that the amplitude of oscillation in a trap will increase as energy is lost. This antidamping is seen in the experiment [18].

Domain walls (often referred to as solitons) are topologically stable in one dimension. Their thickness is set by the coherence length $l_{\rm coh}$ and thus they have a negative effective mass ($-M_{\rm DW}$) due to the density depletion $M_{\rm DW} = mN_{\rm DW}$, where $N_{\rm DW} \sim n\pi R^2 l_{\rm coh}$ is the depletion for a gas cloud of number density n in a trap of radius R. In the unitary limit, all scales are set by the Fermi wave vector k_F with $n = k_F^3/3\pi^2$ and $l_{\rm coh} \sim k_F^{-1}$ and thus, $M_{\rm DW} \sim k_F^2 R^2 m$ is much larger than the mass m of a single fermion. In quantum mechanics, the dynamics of heavy objects is generally well approximated by classical equations of motion. For domain walls, both kinetic and potential energies are localized on the wall; thus, the same mass $M_{\rm DW}$ enters both the kinetic and potential terms and one expects the oscillation period T to be comparable to the natural axial period T_z of the trapping potential. This is confirmed in BEC experiments [22] where $T \approx \sqrt{2}T_z$ and by fermionic simulations [13], where $T \approx \sqrt{3}T_z$.

In contrast, vortex rings [23], which also occur in classical fluids [24], have very different dynamics. In infinite media, for example, with logarithmic accuracy, large rings ($R \gg l_{\rm coh} \sim k_F^{-1}$) have linear momentum $p \sim mn\kappa\pi R^2$, dispersion $\varepsilon(p)$, and speed $v = {\rm d}\varepsilon(p)/{\rm d}p$ [25]

$$\varepsilon \sim \frac{mn\kappa^2 R}{2} \ln \frac{R}{l_{\rm coh}}, \qquad v \sim \frac{\kappa}{4\pi R} \ln \frac{R}{l_{\rm coh}}, \tag{1a}$$

where κ is the circulation. Their speed $v \propto \ln p/\sqrt{p}$ thus *decreases* as the momentum, kinetic energy, and radius increase. Unlike for domain walls, their inertial mass $M_I = F/\dot{v} \sim mn\kappa 8\pi^2 R^3/\ln(R/l_{\rm coh})$, (where $F = \dot{p}$ is the force), differs from the effective mass due to the density depletion $M_{\rm VR} = mN_{\rm VR} \sim mn2\pi^2 R l_{\rm coh}^2$ and the period of oscillation can receive a significant enhancement

$$\frac{T}{T_z} \sim \sqrt{\frac{M_I}{M_{\rm VR}}} \sim \frac{2R/l_{\rm coh}}{\sqrt{\ln(R/l_{\rm coh})}}. \tag{1b}$$

This estimate (1b) gives only an order of magnitude estimate: the dynamics of a vortex ring in a finite trap is somewhat more complicated but can be qualitatively understood. Each element of the ring will experience an outward buoyant force $\boldsymbol{F}_B \approx N_{\rm VR}\nabla V_{\rm trap}$, where $V_{\rm trap} = m\omega_\perp^2(x^2 + y^2 + z^2/\lambda^2)/2$ (with $\lambda > 1$). The Magnus relationship $\boldsymbol{F}_B = mn(\boldsymbol{v} - \boldsymbol{v}_s) \times \boldsymbol{\kappa}$ will thus adjust the velocity $\boldsymbol{v}$ with two components: one counter to $\boldsymbol{v}_s$ and another that causes the ring to expand and contract near the ends of the trap. The velocity $\boldsymbol{v}_s$ is the superflow induced by the phase winding of the rest of the vortex ring on the element, and is parallel to the z axis of the trap. In the middle of the trap $z \approx 0$, small rings (R much less than the trap waist $R_\perp$) will experience little buoyant force and the motion will be dominated by $\boldsymbol{v} \approx \boldsymbol{v}_s$. Larger rings, however, will have a smaller $\boldsymbol{v}_s$ and larger $\boldsymbol{F}_B$: at a critical radius R_c, the Magnus effect will cancel $\boldsymbol{v}_s$ and the ring will remain stationary. Larger rings $R > R_c$ will crawl backwards along the trap. Near the ends of the trap, the buoyant force will also cause the rings to expand at one end and contract at the other. Thus a vortex ring may oscillate along the trap as observed in bosons [26].

Heavy solitons are indeed vortex rings.—While a quantitative discussion requires a more complete analysis along the lines of [27] or direct simulation as we shall present in a moment, the order of magnitude of the effect can be estimated from Eq. (1b) which is approximately valid for small vortex rings near the middle of the trap $z \approx 0$. For the experimental parameters, small rings $R \approx 0.2R_\perp$ (rings with this radius have roughly the same amplitude as the oscillations seen in the experiment) exhibit periods an order of magnitude larger than T_z, naturally explaining the observations. Furthermore, as the system is brought into the BEC regime, the coherence length $l_{\rm coh}$ will grow significantly relative to the fixed ring size R, so T will naturally get smaller, approaching T_z. Finally, in the extreme BEC limit, $l_{\rm coh}$ will approach the width of the trap, arresting the snake instability, and reproducing the theoretical prediction $T \approx \sqrt{2}T_z$ for a domain wall.

Method.—To explain more subtle features of the experiment, like the observed dependence on aspect ratio, we perform dynamical simulations of trapped unitary fermions using two formulations of density functional theory (DFT). The first, an extended Thomas-Fermi (ETF) model [28], is essentially a bosonic theory for the dimer or Cooper-pair wave function Ψ. The dynamics are described by a nonlinear Schrödinger equation (NLSEQ) similar to the Gross-Pitaevskii equation (GPE) for bosons

$$i\hbar\frac{\partial\Psi}{\partial t} = -\frac{\hbar^2}{4m}\nabla^2\Psi + 2\frac{\partial\mathcal{E}_h(n,a)}{\partial n}\Psi + 2V_{\rm ext}\Psi, \tag{2}$$

where arguments $\boldsymbol{x}$ and t have been suppressed, $n = 2|\Psi|^2$ is the fermion number density, and $\mathcal{E}_h(n,a)$ is the energy-density of the homogeneous gas with density n and (adjustable) scattering length a fit to the equation of state in the BEC-BCS crossover. This simplified DFT is equivalent to zero-temperature quantum hydrodynamics (including the so-called quantum pressure term), and we shall use this to model the time-of-flight expansion and imaging procedure of the experiment. While computationally attractive, this formulation has some physical drawbacks. In particular, it models only the superfluid portion of the cloud: physics associated with the normal state is missing. As a result, a vanishing order parameter $\Psi = 0$ implies a vanishing density $n = 0$. This tends to overestimate the density contrast in the core of defects and leads to the same domain wall motion $T \approx \sqrt{2}T_z$ as the harmonically trapped GPE.

There is also no mechanism for the superfluid to transfer energy to the normal component, which inhibits the relaxation of rotating systems into a regular vortex lattice, and prevents Eq. (2) from being used to simulate the preparation of the experiment as the initial sound waves generated by the phase imprint never dampen, and the generated vortex rings rapidly decay.

To address these issues, we also simulate a time-dependent extension of DFT to superfluid systems—the time-dependent superfluid local density approximation (TDSLDA)—where the dynamical evolution is described by equations for the quasiparticle wave functions (u_k, v_k)

$$i\hbar\frac{\partial}{\partial t}\begin{pmatrix} u_k \\ v_k \end{pmatrix} = \begin{pmatrix} h & \Delta \\ \Delta^* & -h \end{pmatrix}\begin{pmatrix} u_k \\ v_k \end{pmatrix}, \tag{3a}$$

where $h = \delta\mathcal{E}/\delta n$ and $\Delta = \delta\mathcal{E}/\delta\nu^*$ (ν is the anomalous density) [29]. This is similar in form to the Bogoliubov–de Gennes (BdG) mean-field theory [13–16], but includes a self-energy contribution β and effective mass parameter α neglected in the BdG:

$$h = \frac{\delta\mathcal{E}}{\delta n} = \alpha\frac{-\hbar^2\nabla^2}{2m} + \beta\frac{(3\pi^2 n)^{2/3}}{2} - \frac{|\Delta|^2}{3\gamma n^{2/3}}. \tag{3b}$$

These additional terms allows the TDSLDA to quantitatively match all experimentally measured and numerically calculated properties of homogeneous systems in finite and infinite boxes [30]: adjusting α, β, and γ allows one to consistently characterize the energy per particle, pairing gap, and quasiparticle spectrum obtained from quantum Monte Carlo (QMC) calculations of the homogeneous infinite system. (Note: If $\alpha \neq 1$, one must include additional terms to restore Galilean covariance as discussed in [29,31]: we avoid this complication by setting $\alpha = 1$ instead of $\alpha \approx 1.1$ while adjusting β and γ to reproduce the energy per particle and pairing gap.) Simulating Eqs. (3) for three-dimensional systems represents a serious computational challenge that effectively utilizes the largest supercomputers available, so we use this only to verify that stable vortex rings are generically produced from the phase-imprint procedure, and use the ETF to illustrate the behavior of the experimental systems.

Results.—Following the preparation procedure outlined in [18], we phase imprint a domain wall on harmonically trapped clouds and follow the evolution using the TDSLDA. (Details are presented in [31].) For sufficiently large clouds, the domain wall quickly decays into an oscillating vortex ring. Figure 1 shows the motion as the ring initially crawls along the outside of the trap and a smaller ring bounces back. Computational limitations restrict us to relatively small systems and these simulations are quite close to the onset of the snake instability. Nevertheless, the period seen in Fig. 1 is comparable to our estimate Eq. (1b). Finally, we note an antidamping similar to that

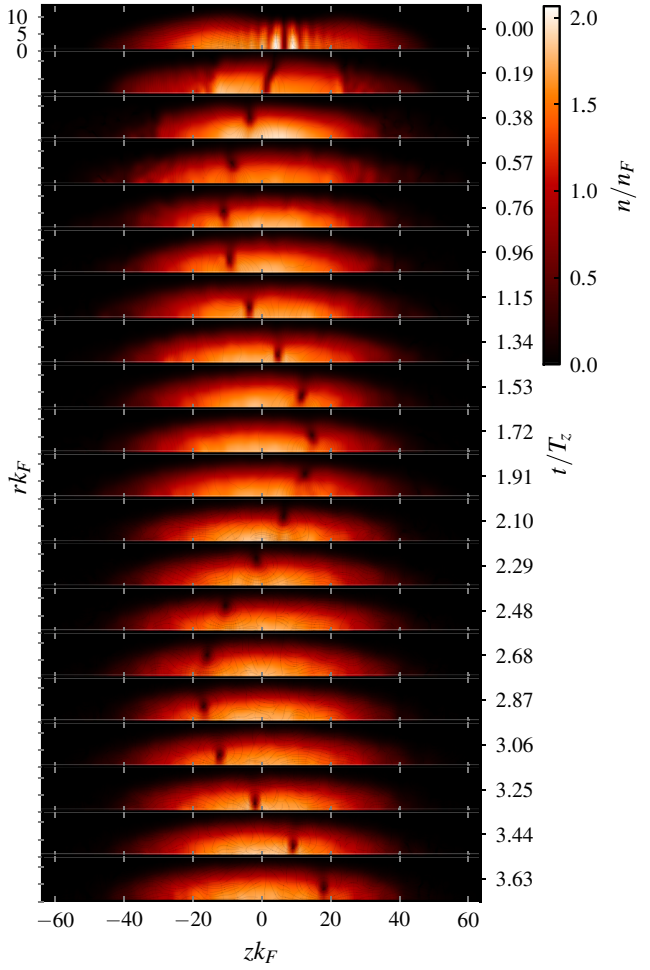

FIG. 1 (color online). Oscillations of a vortex ring in an elongated harmonic trap. Simulated with the TDSLDA on a $32 \times 32 \times 128$ lattice for a cloud with 560 particles. We evolve about 10^5 wave functions in real time using a symplectic split-operator integrator that respects time-reversal invariance using hundreds of GPUs on the Titan supercomputer [32]. More details and several movies may be found in [31].

seen at higher temperatures in [18]. This is explained by the small heat capacity of our simulated system: the residual sound waves induced by the phase correspond roughly to a finite temperature.

For larger clouds we use the ETF . As expected, the initial preparation phase cannot be reliably reproduced: the sound waves generated by the imprint do not dissipate, and the resulting vortex ring decays within a few oscillations. Stable vortex rings can be produced, however, by "cooling" an imprinted phase pattern with imaginary time evolution. As shown in the Supplemental Material [31], these vortex rings reproduce the qualitative behaviors observed in the MIT experiment [18]. In particular, the period is an order of magnitude larger than expected for domain walls and increases by similar amounts as the aspect ratio is reduced as shown in Table I. The period also scales toward the domain wall results $\sqrt{2}T_z$ toward the

TABLE I. Dependence of the oscillation period on aspect ratio for a vortex ring imprinted with $R_0 = 0.30R_\perp$ at resonance. Note that the ETF consistently underestimates the period by about a factor of 0.56.

Aspect ratio	ETF period	Observed period [18]
$\lambda = 3.3$	$T = 9.9T_z$	$T = 18(2)T_z$
$\lambda = 6.2$	$T = 8.4T_z$	$T = 14(2)T_z$
$\lambda = 15$	$T = 6.7T_z$	$T = 12(2)T_z$

BEC limit and exhibits antidamping decays in the presence of phonon excitations. (These phonons mock up fluctuations, but do not faithfully simulate a thermal ensemble.) A quantitative comparison is marred by the lack of a normal component occupying the core of the vortex. However, when comparing the ETF with the TDSLDA simulations, we find that this is fairly consistently characterized by an overall increase in periods by a factor of about 1.8—somewhat larger but similar to the factor of $\approx\sqrt{3/2}$ seen when comparing the period of fermionic to bosonic domain walls in quasi-1D environments. We are confident that a realistic TDSLDA simulation would closely mimic the experiment, and enforcing quantitative agreement would help further constrain the TDSLDA functional.

The puzzle provided by the imaging procedure remains: can a vortex ring look like a planar soliton after imaging? The answer, yes, is demonstrated in Fig. 2 and in [31]. The imaging procedure includes a rapid ramp of the magnetic field to the BEC side of the crossover where the coherence length becomes much larger, but the equation of state becomes softer. This rapid-ramp procedure followed by expansion produces something akin to a shock wave [6,17] that manifests itself as a planar soliton upon imaging. Our simulations confirm the somewhat subtle experimental observation that sufficient ramping below $B_{\min} < 700$ G is required to observe a signal, and explains both the thickness of the soliton and the amplitude of the integrated density fluctuations observed in the experiment [18]. A slight difference remains between the density fringe pattern seen in the integrated 1D density Fig. 2 compared with those seen in experiment [18], the latter having a minimum in the center where the ETF has a peak. As shown in the movies of the expansion [31], this feature results from the motion of shock waves formed during the expansion, the speed of which will be incorrectly predicted by the ETF.

We have shown that the puzzling report of heavy solitons in fermionic superfluids [18], which appear to exhibit an effective mass some 50 times larger than predicted by the theory of dynamics of a domain wall, can be naturally explained in terms of vortex rings. Using a 3D simulation of the TDSLDA, we validate the picture that, in large enough traps, imprinted domain walls generically evolve into vortex rings through an axially symmetric "snake instability. The estimate Eq. (1b) shows that these rings

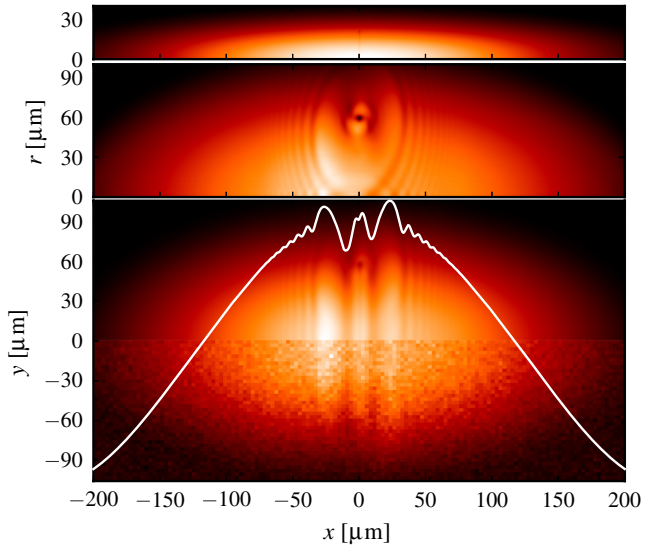

FIG. 2 (color online). Demonstration of the imaging procedure. The top plot shows a slice of the density through the upper-half core of the trap before expansion: the vortex ring is barely visible at $z = 0$. Below is a slice through the upper-half core after ramping to $B_{\min} = 580$ G and letting the cloud expand as discussed [18]. The lower plot shows the integrated 2D density $\int \mathrm{x}\, n(x, y, z)$ and the integrated 1D density $\int \mathrm{x}\, \mathrm{y}\, n(x, y, z)$ (white curve). The lower half of the image has added Gaussian noise with a 3% density variation and is coarse grained on a 3 μm scale to simulate the experimental imaging procedure, clearly demonstrating that vortex rings appear as solitons. (Densities are scaled by maximum value for better contrast.) For $B_{\min} > 700$ G , the density contrast is reduced below the experimental signal-to-noise ratio. See the Supplemental Material [31] for details and for movies.

can have large periods at unitarity, that decreases toward the BEC regime, and explicit simulations using the ETF verify the dependence of the period on the aspect ratio. Finally, the ETF demonstrates that, through the expansion and imaging process employed to resolve the objects, vortex rings manifest as large planar objects with an observable density contrast only if the magnetic field is ramped to $B_{\min} < 700$ G, in quantitative agreement with the observations. We have thus verified virtually all aspects of the experiment [18], including the elaborate imaging protocol, thereby validating the use of the TDSLDA and ETF theories for dynamical simulations including topological defects, and resolving the mystery of heavy solitons as vortex rings.

We acknowledge support under U.S. Department of Energy (DoE) Grants No. DE-FG02-97ER41014 and No. DE-FG02-00ER41132. M. M. K. acknowledges the support provided by an REU NSF fellowship. G. W. acknowledges the Polish Ministry of Science for the support under Contract No. N N202 128439, within the program "Mobility Plus-I edition" under Contract No. 628/MOB/2011/0, and the Polish National Science Center

(NCN) decision No. DEC-2013/08/A/ST3/00708. Some of the calculations reported here have been performed at the University of Washington Hyak cluster funded by the NSF MRI Grant No. PHY-0922770. This research also used resources of the National Center for Computational Sciences at Oak Ridge National Laboratory, which is supported by the Office of Science of the DOE under Contract No. DE-AC05-00OR22725. We thank R. Sharma and M. Zwierlein for discussions.

[1] *The BCS–BEC Crossover and the Unitary Fermi Gas*, edited by W. Zwerger, Lecture Notes in Physics Vol. 836 (Springer–Verlag, Berlin, Heidelberg, 2012).
[2] M. Bartenstein, A. Altmeyer, S. Riedl, S. Jochim, C. Chin, J. H. Denschlag, and R. Grimm, Phys. Rev. Lett. **92**, 203201 (2004); A. Altmeyer, S. Riedl, M. J. Wright, C. Kohstall, J. H. Denschlag, and R. Grimm, Phys. Rev. A **76**, 033610 (2007); M. J. Wright, S. Riedl, A. Altmeyer, C. Kohstall, E. R. Sánchez Guajardo, J. H. Denschlag, and R. Grimm, Phys. Rev. Lett. **99**, 150403 (2007); S. Riedl, E. R. Sánchez Guajardo, C. Kohstall, A. Altmeyer, M. J. Wright, J. H. Denschlag, R. Grimm, G. M. Bruun, and H. Smith, Phys. Rev. A**78**, 053609 (2008).
[3] J. Kinast, S. L. Hemmer, M. E. Gehm, A. Turlapov, and J. E. Thomas, Phys. Rev. Lett. **92**, 150402 (2004); J. Kinast, A. Turlapov, and J. E. Thomas, Phys. Rev. A **70**, 051401 (2004).
[4] E. R. S. Guajardo, M. K. Tey, L. A. Sidorenkov, and R. Grimm, Phys. Rev. A **87**, 063601 (2013).
[5] M. W. Zwierlein, J. R. Abo-Shaeer, A. Schirotzek, C. H. Schunck, and W. Ketterle, Nature (London) **435**, 1047 (2005).
[6] J. A. Joseph, J. E. Thomas, M. Kulkarni, and A. G. Abanov, Phys. Rev. Lett. **106**, 150401 (2011).
[7] J. Joseph, B. Clancy, L. Luo, J. Kinast, A. Turlapov, and J. E. Thomas, Phys. Rev. Lett. **98**, 170401 (2007).
[8] D. E. Miller, J. K. Chin, C. A. Stan, Y. Liu, W. Setiawan, C. Sanner, and W. Ketterle, Phys. Rev. Lett. **99**, 070402 (2007).
[9] M. K. Tey, L. A. Sidorenkov, E. R. Sánchez Guajardo, R. Grimm, M. J. H Ku, M. W. Zwierlein, Y.-H. Hou, L. Pitaevskii, and S. Stringari, Phys. Rev. Lett. **110**, 055303 (2013); L. A. Sidorenkov, M. K. Tey, R. Grimm, Y.-H. Hou, L. Pitaevskii, and S. Stringari, Nature (London) **498**, 78 (2013).
[10] A. Bulgac and S. Yoon, Phys. Rev. Lett. **102**, 085302 (2009).
[11] R. G. Scott, F. Dalfovo, L. P. Pitaevskii, and S. Stringari, Phys. Rev. A **86**, 053604 (2012).
[12] A. Bulgac, Y.-L. Luo, P. Magierski, K. J. Roche, and Y. Yu, Science **332**, 1288 (2011).
[13] R. G. Scott, F. Dalfovo, L. P. Pitaevskii, and S. Stringari, Phys. Rev. Lett. **106**, 185301 (2011).
[14] M. Antezza, F. Dalfovo, L. P. Pitaevskii, and S. Stringari, Phys. Rev. A **76**, 043610 (2007).
[15] A. Spuntarelli, L. D. Carr, P. Pieri, and G. C. Strinati, New J. Phys.**13**, 035010 (2011).
[16] R. Liao and J. Brand, Phys. Rev. A **83**, 041604 (2011).
[17] A. Bulgac, Y.-L. Luo, and K. J. Roche, Phys. Rev. Lett. **108**, 150401 (2012).
[18] T. Yefsah, A. T. Sommer, M. J. H Ku, L. W. Cheuk, W. Ji, W. S. Bakr, and M. W. Zwierlein, Nature (London) **499**, 426 (2013).
[19] W. F. Vinen and J. J. Niemela, J. Low Temp. Phys. **128**, 167 (2002); W. F. Vinen, J. Low Temp. Phys. **145**, 7 (2006); W. F. Vinen, J. Low Temp. Phys. **161**, 419 (2010); L. Skrbek, J. Phys. Conf. Ser. **318**, 012004 (2011); M. Tsubota, J. Phys. Soc. Jpn. **77**, 111006 (2008); M. Tsubota, M. Kobayashi, and H. Takeuchi, Phys. Rep. **522**, 191 (2013); M. S. Paoletti and D. P. Lathrop, Annu. Rev. Condens. Matter Phys. **2**, 213 (2011).
[20] A. Bulgac and Y. Yu, Phys. Rev. Lett. **91**, 190404 (2003).
[21] Y. Yu and A. Bulgac, Phys. Rev. Lett. **90**, 161101 (2003).
[22] C. Becker, S. Stellmer, P. Soltan-Panahi, S. Dorscher, M. Baumert, E.-M. Richter, J. Kronjager, K. Bongs, and K. Sengstock, Nat. Phys. **4**, 496 (2008); A. Weller, J. P. Ronzheimer, C. Gross, J. Esteve, M. K. Oberthaler, D. J. Frantzeskakis, G. Theocharis, and P. G. Kevrekidis, Phys. Rev. Lett. **101**, 130401 (2008).
[23] G. W. Rayfield and F. Reif, Phys. Rev. **136**, A1194 (1964).
[24] H. Lamb, *Hydrodynamics* (Dover, New York, 1945), 6th ed.; P. Saffman, *Vortex Dynamics* (Cambridge University Press, Cambridge, England, 1992).
[25] P. Roberts and R. Donnelly, Phys. Lett. **31A**, 137 (1970); C. F. Barenghi and R. J. Donnelly, Fluid Dyn. Res. **41**, 051401 (2009).
[26] I. Shomroni, E. Lahoud, S. Levy, and J. Steinhauer, Nat. Phys. **5**, 193 (2009).
[27] S. Komineas, Eur. Phys. J. Spec. Top. **147**, 133 (2007).
[28] Y. E. Kim and A. L. Zubarev, Phys. Lett. A **327**, 397 (2004); Y. E. Kim and A. L. Zubarev, Phys. Rev. A **70**, 033612 (2004); L. Salasnich, F. Ancilotto, N. Manini, and F. Toigo, Laser Phys. **19**, 636 (2009); L. Salasnich and F. Toigo, Phys. Rev. A **78**, 053626 (2008); L. Salasnich and F. Toigo, Phys. Rev. A **82**, 059902(E) (2010).
[29] A. Bulgac, M. M. Forbes, and P. Magierski, in *The BCS-BEC Crossover and the Unitary Fermi Gas*, edited by W. Zwerger, Lecture Notes in Physics Vol. 836 (Springer, New York, 2012), Chap. 9, p. 305; A. Bulgac, Annu. Rev. Nucl. Part. Sci. **63**, 97 (2013).
[30] M. M. Forbes, S. Gandolfi, and A. Gezerlis, Phys. Rev. A **86**, 053603 (2012).
[31] See Supplemental Material at http://link.aps.org/supplemental/10.1103/PhysRevLett.112.025301 for details about our numerical calculations, movies, and figures with finer resolution. Additional movies are available at: http://www.phys.washington.edu/~bulgac/media_files/VR
[32] http://www.olcf.ornl.gov/computing-resources/titan-cray-xk7/.